# RSC Advances


Cite this: DOI: 10.1039/c0xx00000x

www.rsc.org/advances

PAPER

# Highly selective $NO_2$ sensor at room temperature based on the nanocomposites of hierarchical nanosphere-like α-$Fe_2O_3$ and reduced graphene oxide†

**Ying-li Dong, Xian-fa Zhang, Xiao-li Cheng, Ying-ming Xu*, Shan Gao, Hui Zhao, Li-hua Huo***

***Received (in XXX, XXX) Xth XXXXXXXXX 201X, Accepted Xth XXXXXXXXX 201X***
**DOI: 10.1039/b000000x**

Nanosphere-like α-$Fe_2O_3$ modified reduced graphene oxide nanosheets have been prepared by a simple hydrothermal method without any surfactant or template. The nanocomposites have been characterized by using X-ray diffraction (XRD), Raman spectra (RS), Fourier transform infrared (FT-IR) spectra, X-ray photoelectron spectroscopy (XPS), scanning electron microscopy (SEM) and transmission electron microscopy (TEM) techniques. α-$Fe_2O_3$ nanospheres are hierarchical structure with the diameter of about 40～50 nm and grow on the surface of the single graphene nanosheets uniformly. α-$Fe_2O_3$/rGO nanocomposites exhibit high response of 150.63% to 90 ppm $NO_2$ at room temperature, which is raised by 65.5 times as compared to that of pure graphene, and the detection limit of $NO_2$ can be decreased down to 0.18 ppm. Sensing mechanism of the nanocomposites to $NO_2$ was proposed. The high response of the nanocomposites to $NO_2$ at room temperature is the synergistic effect of these two sensing materials and large specific surface area of the nanocomposites.

## Introduction

Carbon materials, due to its all kinds of excellent properties, such as cost-effectiveness, environmental friendliness, availability and corrosion resistance,[1] have always been favourite research object for scientists. As the thinnest material, graphene has walked into the stage of nanomaterials formally since 2008 due to its outstanding physical and chemical properties, and has been widely used in supercapacitor, Li-ion batteries, gas sensors and so on.[1-4] In comparison to other gas sensing materials, graphene has the following advantages in the field of gas sensors: excellent conductivity, very large specific surface area, exceptional low noise to signal ratios, and low working temperature. Graphene has been investigated to detect the gases including $NO_2$, $NH_3$, $H_2O$ and CO.[5-7]

However, graphene happens to reunite among sheets due to the effect of van der Waals interactions, leading to low sensitivity and irreversibility of the sensors.[8,9] In order to overcome these problems, organic functional groups (sulfonated, ethylenedia-mine)[10] and noble metals (Pd,[11] Au,[12] Ag[12]) have been once investigated as the modified materials. Recently, semiconducting metal oxides have been chosen as the modified materials such as $SnO_2$,[13] NiO,[14] $WO_3$,[15] ZnO,[16] $Fe_2O_3$,[17] due to their easy synthesis, low cost and good stability. These composites exhibit high sensitivity and reversibility at the working temperature of 150～300℃. Some metal oxides/graphene composites have been also investigated to decrease the working temperature, and they show certain response to some test gases at room temperature. For example, $Cu_2O$ nanowire,[18] $Co_3O_4$ nanoparticles,[19] $SnO_2$ nanoparticles[20] and indiumdoped $SnO_2$ nanoparticles[21] have been studied to modify reduced graphene oxide which exhibit certain responses with long response-recovery characteristics to $NO_2$. Radial flower-like $SnO_2$,[22] ZnO quantum dots,[23] $TiO_2$ nanoparticles[24] and $Cu_2O$ nanoparticles[25] have been also considered to be composited with graphene to detect $NH_3$, HCHO, $O_2$ and $H_2S$ respectively but with low responses at room temperature. However, the selectivity of most nanocomposite materials was not investigated in the above reports. It is interesting to explore new nanocomposites which show good selectivity to the target gases at room temperature.

Ferric oxide nanomaterials are a kind of functional material whose composites with graphene have been applied mainly in Li-ion batteries,[26] frictional materials,[27] high-performance catalyst,[28] supercapacitor,[29] biosensor[30] and so on. Only two studies of $Fe_2O_3$-graphene nanocomposites used in the gas sensors at high temperature were recently reported. Liang et al. prepared α-$Fe_2O_3$ nanoparticles modified graphene nanocomposites at 180℃ via an ethanol solvothermal route, which showed response of about 29 to 1000 ppm ethanol at 280℃.[17] Another paper-like $Fe_2O_3$ nanoparticles coated graphene nanosheets were obtained by a super critical $CO_2$ assisted thermal method followed by vertical magnetic field assembly with directed flow. The material exhibits a CL emission of about 450 absorption units in response to 15 ppm $H_2S$ at 190℃ with good selectivity.[31] Consideration of our previous investigation, the working temperature of the sensors could be decreased down to room temperature when the microstructure of the sensing materials was controlled through construction of the 3D hierarchical structure[32] or adjustment of special morphology.[33] If hierarchical α-$Fe_2O_3$ nanomaterial with special morphology was used to modified graphene, the working temperature of such nanocomposites might be decreased.

With the fast development of automobile industry, nitrogen dioxide, produced mainly by automobiles and power plants, has been one of the main pollutants in the atmospheric environment. It is well known that $NO_2$ can destroy the ozone layer, it can also do great harm to human health, e.g. respiratory system of human. According to reports, the Lethal Concentration 50 (LC50) of $NO_2$ is 126 mg/m$^3$, the exposure time is no longer than 8 h to 3 ppm $NO_2$. [21] So it is a challenge to develop efficient sensors to selectively detect low concentrations of $NO_2$ in a short time at low temperature.

In this paper, we report a simple and low cost hydrothermal synthesis route to prepare α-$Fe_2O_3$/rGO nanocomposites at 120℃, in which nanosphere-like α-$Fe_2O_3$ of 40～50 nm diameter are constructed by a few nanometer sized nanoparticles and reduced graphene oxide (rGO) are intercalated single sheets. This nanocomposites exhibit excellent response and selectivity to $NO_2$ at room temperature.

## Experimental

### Preparation of α-$Fe_2O_3$/rGO nanocomposites

All the materials were used of analytical grade in this work. 20 mg graphene oxide (GO) was prepared by natural flake graphite (325 mesh) according to the modified Hummers method,[34] was dispersed in 20 mL deionized water and sonicated for 1 h. 10 mL 0.022 mol·L$^{-1}$ $FeCl_3$ aqueous solution was added dropwise into the above GO disperse solution with magnetically stirring for 30 min and sonicated for 10 min. The solution was transferred into a Teflonlined autoclave and maintained at 120℃ for 8 h. The final product of α-$Fe_2O_3$/rGO nanocomposites was obtained after vacuum filtration, washed with deionized water, and dried at 60 ℃, as shown in Fig. 1a. Reduced graphene oxide (rGO) and pure α-$Fe_2O_3$ nanoparticles were also obtained through a similar procedure only in the absence of $FeCl_3\cdot 6H_2O$ and GO correspondingly.

**Fig. 1 The experimental reaction diagram of α-$Fe_2O_3$/rGO nanocomposites (a), schematic of α- $Fe_2O_3$/rGO nanocomposites on the sensor substrate (b) and schematic of sensing test (c).**

### Characterizations

The composition and phase purity of the as-synthesized samples were analyzed by powder X-ray diffractometer (XRD) with monochromatized Cu Kα (λ=0.15406 nm) by a Rigaku, D/MAX-3B instrument operating at 40 kV voltage and 50 mA current. The nanocomposites were analyzed using a Renishaw 1000 Micro-Raman spectrometer using a long-range 50×objective, 10S integration, and 10% laser power (457.9 nm excitation; 8 mW at 100%). The chemical compositions on the surface of nanocomposites were detected by Fourier transform infrared (FT-IR) spectroscopy (Nexus, Thermo Nicolet). The sample was also analyzed by X-ray photoelectron spectroscopy (XPS, Kratos, ULTRA AXIS DLD) with monochromatized Al Kα (hν=1486.6 eV) radiation. All binding energies were calibrated by referencing to C1s (284.6 eV). The size and morphology of the samples were observed by field emission scanning electron microscope (FESEM, FEI/Philips, XL-30). A JEM-2010 transmission electron microscope (TEM), operating at a 200 kV accelerating voltage, was used for TEM analysis. Specific surface area of the products was analyzed by nitrogen adsorption–desorption at 77 K using a Gas Sorption System (Micro-metrics Instruments, TriStar II 3020).

### Gas sensor fabrication and sensing measurements

To prepare gas sensors composed of α-$Fe_2O_3$/rGO nanocomposites, 18 pairs of gold interdigitated electrodes were fabricated by an e-beam lithography process on a $Al_2O_3$ wafer. The size of wafer is 9.4×9.4×0.38 mm on which the distance of electrodes is 50 μm. The α-$Fe_2O_3$/rGO nanocomposites were dispersed in ethanol to form dispersion liquid, which (75 μL, 1.53×10$^{-6}$g/μL) was dropped on the gold electrode of the sensor substrate uniformly by spin coating, as shown in Fig. 1b. To volatilize the solvent completely, the sensor devices were dried at 100℃ for 10 min before sensing measurements.

The gas-sensing properties of the nanocomposites sensors were tested in a closed container at room temperature (ca. 25℃) by a dynamic gas test method with a gas inlet and a gas outlet using JF02E type gas sensor tester (Kunming, China). The different concentrations of test gas were obtained through mixing test gas and dry air, all from standard bottles and controlled by the mass flow controllers. The certain concentration of test gas was controlled at a constant rate of 200 standard cubic centimeter (sccm) per minute during the testing process as shown in Fig. 1c.

The sensitive degree of the sensors was detected by the change of the sensor resistance, and the changes were collected through a computer. To begin the sensing measurement, the sensors were put into the closed container, firstly the dry air flow was flowed into the container to keep the container clean. Then the test gas was flowed into the container, the changes of signals were collected by a computer during the gas passing. After 80 s, the test gas flow was stopped, only the dry air was kept circulating in the whole container. The response is defined as S= [(Ra-Rg)/Rg] ×100%, in which Ra is the resistance of the sensors in the dry air flow and Rg is the resistance of the sensors in the test gas. Due to the long recovery time of graphene materials,[6,35,36] the response time is controlled as 80 s. The recovery time is defined as the time needed to reach 63% of total signal change.

In order to investigate the influence of the humidity on the gas sensing property of the nanocomposites, the responses of the nanocomposites to different relative humidities (11.3～75.3% RH) were also tested by a static gas test method. The test method is consistent with the literature.[37] Table 1 shows standard equilibrium relative humidity at the confined space on the top of saturated salt solutions at room temperature (25 ℃). [37]

**Table 1 Standard equilibrium relative humidity at the confined space on the top of saturated salt solutions at room temperature (25 ℃).**

## Results and discussion

### Characterization of α-$Fe_2O_3$/rGO nanocomposites

Fig. 2 shows the XRD patterns of α-$Fe_2O_3$/rGO nanocomposites and graphene oxide. There is only one obvious peak centered at 2θ=10.0° in Fig. 2b, corresponding to the (002) interplanar spacing of 0.9235 nm of graphene oxide.[38] After α-$Fe_2O_3$ composited with GO, a few sharp diffraction peaks appear at 2θ of 24.1°, 33.2°, 35.6°, 40.8°, 49.5°, 54.1°, 62.5° and 64.1° corresponding to (012), (104), (110), (113), (024), (116), (214) and (300) crystal planes of hematite phase, respectively in Fig. 2a, which can be indexed to rhombohedral structure of α-$Fe_2O_3$ (JCPDS no.33-0664). No characteristic diffraction peak of graphite oxide can be seen, illustrating that the GO in the nanocomposites has been reduced completely. No peaks corresponding to any impurities are detected.

**Fig. 2 XRD patterns of α-$Fe_2O_3$/rGO nanocomposites (a) and graphene oxide (b).**

**Fig. 3 Raman spectra of graphene oxide (a), reduced graphene oxide (rGO) (b) and α-$Fe_2O_3$/rGO nanocomposites (c).**

Characteristics of carbon materials can be distinguished well by Raman spectra. In the carbon materials, the in-plane vibration of C $sp^2$ atoms corresponds to G band, which locates at about 1587 $cm^{-1}$, disorders and defects of the graphitic layer correspond to D band, which locates at about 1330 $cm^{-1}$.[39] The intensity ratio of D/G (ID/IG) indicates disorder and defect structures and defect density of carbon materials.[39,40] Fig. 3 shows the Raman spectra of graphene oxide (a), rGO (b) and α-$Fe_2O_3$/rGO nanocomposites (c), which show similiar G band and D band, indicating the existence of carbon material in the nanocomposites. The ID/IG ratio increases from 0.7325 for GO to 0.8630 for rGO, suggesting the higher defects and disorders of rGO. This is because more functional groups were dropped out when graphene oxide was reduced to rGO. However, the ID/IG ratio of α-$Fe_2O_3$/rGO nanocomposites is the highest (0.9834) in the three materials, indicating the highest defects and disorders of carbon material in the nanocomposites, which might be further resulted from the α-$Fe_2O_3$ nanoparticles modified on the surface of rGO.

**Fig. 4 FT-IR spectra of graphene oxide (a), rGO (b) and α-$Fe_2O_3$/rGO nanocomposites (c).**

Fig. 4 shows the FT-IR spectra of the nanocomposites and related single materials. The FT-IR spectrum of graphene oxide (Fig. 4a) displays the characteristic absorption bands for the stretching vibration of hydroxyl groups (3376 $cm^{-1}$), the stretching vibration of water molecules (3141 $cm^{-1}$) , the stretching vibration of carboxyl groups on the edges of the layer planes or conjugated carbonyl groups (1719 $cm^{-1}$),[41] the vibration of carboxyl C–O (1417 $cm^{-1}$), epoxy C–O (1223 $cm^{-1}$) and alkoxyl C–O (1053 $cm^{-1}$) of graphene oxide.[28] The band, located at 1621$cm^{-1}$ might be from skeletal vibration of unoxidized graphitic domains.[42] In the FT-IR spectrum of rGO (Fig. 4b), there are three bands at 1719 (C=O),[41] 1580 (C=C)[43] and 1223 $cm^{-1}$ (epoxy C–O), but other functional groups from graphene oxide disappear. These changes suggest that graphene oxide was reduced completely by our synthetic method. For the case of the nanocomposites (Fig. 4c), the absorption bands of 1719 $cm^{-1}$ (C=O), 1580$cm^{-1}$ (C=C) and 1223 $cm^{-1}$ (epoxy C–O) are also found, suggesting that rGO in deed existed in the nanocomposites. In addition, there are two strong absorption bands located at 550 and 470 $cm^{-1}$ (Fig. 4c), which are the characteristic Fe-O vibration in α-$Fe_2O_3$ nanomaterial.[44] In conclusion, FT-IR spectra analysis also confirms that the product is α-$Fe_2O_3$/rGO nanocomposites.

**Fig. 5 XPS spectra of full survey (a), the fine spectrum of Fe2p (b), the fine spectrum of C 1s of graphene oxide (c), reduced graphene oxide (d) and α-$Fe_2O_3$/rGO nanocomposites (e).**

To research the surface compositions and chemical states of α-$Fe_2O_3$/rGO nanocomposites, XPS analysis of the nanocomposites was carried out (Fig. 5). The XPS full survey spectrum (Fig. 5a) indicates that the nanocomposites contain O, Fe and C elements with sharp peaks locating at binding energies of 973.5 (auger electron peak of O), 898.3, 884.0, 786.2 (auger electron peak of Fe), 847.1 (Fe2s), 724.5 (Fe2p), 531.6 (O 1s), 284.6 (C 1s), 98.5 (Fe3s), and 55.6 eV (Fe3p), respectively.

The fine spectrum of Fe2p (Fig. 5b) shows the chemical state of Fe. Two distinct wide peaks, located at binding energies of 713.3 and 726.2 eV for Fe 2p3/2 and Fe 2p1/2 respectively, are characteristic of $Fe^{3+}$ specie in $Fe_2O_3$ which are in good agreement with previous reports.[45,46]

To gain further insights into chemical states and changes of C elements in α-$Fe_2O_3$/rGO nanocomposites, the fine spectra of C 1s of graphene oxide, rGO and the nanocomposites are compared. As shown in Fig. 5c, four wide peaks can be observed in the fine spectrum of C 1s of graphene oxide, which locate at 284.3, 286.4, 287.6 and 288.6 eV, corresponding to C-C, C-O (epoxy and alkoxy), C=O (carbonyl) and O-C=O (carboxyl) of GO, respectively.[47] Table 2 shows the percent content of chemical states of C 1s in three materials. As can be seen, the percent content of C-O is the highest in graphene oxide, this is because many epoxy, alkoxy, carbonyl and carboxyl groups exist on the surface of graphene oxide.

After graphene oxide was reduced, four wide peaks are observed in the fine spectrum of C 1s of rGO, locating at 284.6, 286.0, 287.3, and 288.6 eV (Fig. 5d). The binding energy positions are similar with those of GO. However, the percent content of C-C is the highest in rGO, the percent contents of the rest of the valence bonds decrease (see Table 2), in comparison with those of GO. That is the numbers of epoxy, alkoxy and carboxyl groups on the edges of rGO decrease, resulted from the deoxygenation and reduction of graphene oxide, which confirms the consequence of FT-IR analysis.

From the fine spectrum of C 1s in the nanocomposites (Fig. 5e), four wide peaks are also seen at 284.6, 286.0, 287.5, and 288.9 eV, which are consistent with those of rGO. The percent contents of all oxygen-containing functional groups in the nanocomposites increase, but the percent content of C-C is still the highest. It indicates that there are obvious bonding interaction between the modified α-$Fe_2O_3$ particles and carbon material, which preserving some oxygen-containing functional groups in the composites, although GO is reduced during the nanocomposites synthesis. This is consistent with the above analysis results.

**Table 2 The percent contents of chemical states of C 1s (%) in graphene oxide, rGO and α-$Fe_2O_3$/rGO nanocomposites.**

**Fig. 6 SEM images of reduced graphene oxide (a) and α-$Fe_2O_3$/rGO nanocomposites (b). TEM images of α-$Fe_2O_3$/rGO nanocomposites (c-d).**

The morphology of the α-$Fe_2O_3$/rGO nanocomposites and the distribution of the oxide on the rGO layer can be observed from SEM (Fig. 6b) and TEM (Fig. 6c～d) images. It can be seen that the oxide particles uniformly distribute on the surface of rGO layer (Fig. 6b). They are irregular hierarchical sphere-like assembly with the size of about 40～50 nm, which are further constructed by a few nanometer sized smaller particles (Fig. 6d). In comparison with the pure rGO (Fig. 6a), the monolayer of rGO can be clearly seen in the nanocomposites (Fig. 6b～d). It indicates that the existence of α-$Fe_2O_3$ nanospheres well prevents the reunion of rGO layers. This will be benefit for the nanocomposites to adsorb and react with the test gas.

**Fig. 7 Nitrogen adsorption–desorption isotherm of α-$Fe_2O_3$/rGO nanocomposites.**

The surface information of the α-$Fe_2O_3$/rGO nanocomposites was further obtained by the nitrogen adsorption and desorption measurements. Fig. 7 shows the representative $N_2$ adsorption and desorption isotherms of the nanocomposites. The specific surface area of the nanocomposites was calculated to be 193.15 $m^2g^{-1}$ by the Brunauer–Emmett–Teller (BET) method. The measured value is larger than that of rGO (120.20 $m^2g^{-1}$). This is because the existence of α-$Fe_2O_3$ nanospheres well prevents the reunion of rGO layers.

## Gas sensing property of the nanocomposites

**Fig. 8 (a) Exponential curve of response of the nanocomposites as a function of $NO_2$ concentration. (b) Dynamic responses of α-$Fe_2O_3$/rGO nanocomposites to different concentrations of $NO_2$. (c) Response comparison of α-$Fe_2O_3$/rGO nanocomposites, reduced graphene oxide and α-$Fe_2O_3$ to 18～90 ppm $NO_2$. (d) Response comparison of α-$Fe_2O_3$/rGO nanocomposites, reduced graphene oxide and α-$Fe_2O_3$ to different gases at room temperature.**

Fig.8a shows the responses of α-$Fe_2O_3$/rGO nanocomposites to a series of concentrations of $NO_2$ at room temperature. With the concentration of $NO_2$ increasing, the responses of the nanocomposites increase and there are nearly linear relationships in the concentration ranges of 0.18～9 ppm ($R^2$=0.99017) and 9～90 ppm ($R^2$=0.99151). After flowing into 54 ppm $NO_2$ for 80s, an 88.27% response increment can be observed, which is much larger than that of $SnO_2$/rGO composites (6.5%, 50 ppm) [20] and a little larger than $Co_3O_4$/rGO composites (80%, 60 ppm)[19] to $NO_2$, The nanocomposites can detect as low concentration of $NO_2$ as 0.18 ppm.

Fig.8b shows dynamic responses of α-$Fe_2O_3$/rGO nanocomposites to 0.18～90 ppm $NO_2$. The recovery time of α-$Fe_2O_3$/rGO nanocomposites was in the range of 44～1648 s. The recovery time is 44 s when the concentration of $NO_2$ was 0.18 ppm.

In order to compare gas responses of the α-$Fe_2O_3$/rGO nanocomposites, reduced graphene oxide and pure α-$Fe_2O_3$ sensors were also fabricated using the same conditions and the sensing properties were tested to a series of gases under the same conditions at room temperature (Fig.8c～d). As shown in Fig.8c, rGO and α-$Fe_2O_3$ sensors are almost insensitive to $NO_2$ within 54 ppm of concentration. Only increasing the $NO_2$ concentration to 90 ppm, rGO sensor exhibits 2.29% response to $NO_2$, which is still much lower than the nanocomposites sensor (150.63%). It indicates better sensing property of nanocomposites to $NO_2$ than single sensing materials.

Fig.8d shows the responses of the three materials to $NO_2$ (54 ppm), CO (54 ppm), HCHO (54 ppm), $H_2S$ (0.1%), $NH_3$ (0.1%) and $C_2H_5OH$ (54 ppm). The three sensors are almost all insensitive to CO and HCHO, but show low and similar responses to $H_2S$, $NH_3$ and $C_2H_5OH$, in which the nanocomposites are a little more sensitive to $H_2S$ (4.56%) than the others, the nanocomposites and rGO show similar and a little larger responses (4.4%) to $NH_3$ than α-$Fe_2O_3$, and α-$Fe_2O_3$ exhibits twice times of response (6.96%) than rGO and nanocomposites sensors to $C_2H_5OH$. However, all the responses of the three sensors to these three gases were neglected in comparison with that of nanocomposites to $NO_2$. The selectivity coefficients of the nanocomposites to $NO_2$ and other gases are in the range of 19.34～275.8. It indicates that the nanocomposites show excellent selectivity to $NO_2$ at room temperature.

**Fig. 9 Responses of α-$Fe_2O_3$/rGO nanocomposites to humidity from 11.3 to 75.3% RH at room temperature.**

Fig. 9 shows the responses of α-$Fe_2O_3$/rGO nanocomposites to the humidity from 11.3 to 75.3% RH at room temperature. It can be seen that the relative responses of the nanocomposites to the humidity in the whole measured range are 0～86.48%. It means that the low humidity ( < 54.4% RH) has no obvious effect on the $NO_2$ gas (90 ppm) sensing property of the nanocomposites. Even in high humidity (75.3% RH), the nanocomposites still exhibit almost twice times of response to $NO_2$ (90 ppm) than that to humidity (75.3% RH). So the influence of water vapors on the $NO_2$ gas sensing property of the nanocomposites could be neglected in this study.

## $NO_2$ sensing mechanism of the nanocomposites

**Fig. 10 Proposed sensing mechanism of α-$Fe_2O_3$/rGO nanocomposites to $NO_2$.**



 

rGO possesses p-type semiconductor characteristics.[6] The sensing mechanism of rGO to $NO_2$ (oxidizing gas) can be described as follows: $NO_2$ captures an electron from rGO, which leads to the increase of hole density, resulting in the resistance of rGO decrease.[48] The reaction can be illustrated as follows:

$NO_2\,(gas) + e^- \leftrightarrow NO_2^-$ (1).

α-$Fe_2O_3$ is well known a n-type semiconductor with oxygen vacancies or metal ions as electron donors. The oxygen molecules in air act as acceptors by trapping electrons from the α-$Fe_2O_3$ conduction band, become chemisorbed oxygen $O_2^-$ (<100℃) on the surface of sensing material,[49] which are illustrated as follows:

$O_2\,(gas) \rightarrow O_2\,(ads)$ (2).

$O_2\,(ads) + e^- \rightarrow O_2^-\,(ads)$ (<100 ℃) (3).

However, pure α-$Fe_2O_3$ is almost insensitive to $NO_2$ at room temperature. After α-$Fe_2O_3$ composited with rGO, α-$Fe_2O_3$/rGO nanocomposites exhibit good response to $NO_2$, which might be explained by the following sensing mechanism:

When α-$Fe_2O_3$/rGO nanocomposites are exposed to $NO_2$ (shown in Fig. 10), an electron of rGO is captured by $NO_2$, which leads to the decrease of resistance. At the same time, $NO_2$ reacts with $O_2^-$ (ads) on the surface of α-$Fe_2O_3$ of the nanocomposites, forming an intermediate complex $NO_3^-$.[50] The reaction between $O_2^-$(ads) on the surface of α-$Fe_2O_3$ and $NO_2$ molecules can be described as follows:

$2NO_2\,(gas) + O_2^-(ads) \rightarrow 2\,NO_3^-(ads)$ (4).

The reaction of $NO_2$ and $O_2^-$ (ads) leads to unbalance of charge on the surface of α-$Fe_2O_3$. rGO provides more electrons to α-$Fe_2O_3$ to form $O_2^-$(<100 ℃) on the surface of α-$Fe_2O_3$, in consequence more holes produce in rGO resulting in the decrease of the nanocomposites resistance.

When the nanocomposites are exposed to air again, $NO_2$(ads) species desorb with leaving the electrons to the nanocomposites. Electrons combine with holes again, which makes the resistance of the nanocomposites increase to the starting value.

In addition, there is another possible reason to explain such excellent sensing property of the nanocomposites to $NO_2$ at room temperature: Uniformly distributed α-$Fe_2O_3$ nanospheres can separate rGO layers perfectly, especially these nanospheres are hierarchical nanostructure which are further assembled by a few nanometer sized particles. The specific surface area of the composites increases greatly compared with that of rGO, which is benefit for more $NO_2$ molecules to adsorb and react on the surface of the nanocomposites. As a consequence, the nanocomposites exhibit high response to $NO_2$.

## Conclusions

Hierarchical nanosphere-like α-$Fe_2O_3$ have been used to modify reduced graphene oxide nanosheets by a simple hydrothermal method without any surfactant or template. α-$Fe_2O_3$ nanospheres distribute uniformly on the surface of rGO single sheets. Because of modification of α-$Fe_2O_3$ nanospheres, the response of the rGO has been improved greatly. The gas sensing responses of the resulting nanocomposites demonstrate that α-$Fe_2O_3$/rGO nanocomposites significantly enhance the response to $NO_2$ comparing with pure graphene and α-$Fe_2O_3$ at room temperature. The synergistic effect of these two single sensing materials and large specific surface area of the nanocomposites lead to the high response of the nanocomposites to $NO_2$ at room temperature. Because of simple preparation method, inexpensive experiment cost and high response and selectivity, the α-$Fe_2O_3$/rGO nanocomposites have a commendable application prospect in the $NO_2$ sensor.

## Acknowledgments

This work is supported by the National Natural Science Foundation of China (61271126, 21201060 and 21305033), Program for Innovative Research Team in University (IRT-1237), Heilongjiang Educational Department (2013TD002, 2011CJHB006, 12541613), Youth Foundation of Harbin (2013RFQXJ142).

## Notes and references

*Key Laboratory of Functional Inorganic Material Chemistry, Ministry of Education, School of Chemistry and Materials Science, Heilongjiang University, Harbin 150080, People's Republic of China. E-mail address: lhhuo68@yahoo.com; Tel.: (+86) 0451-86608426; Fax: (+86) 0451-86608040.*


1 S. Basu and P. Bhattacharyya, Sens. Actuators, B, 2012, 173, 1.
2 K. Zhang, L. L. Zhang, X. S. Zhao and J. S. Wu, Chem. Mater., 2010, 22, 1392.
3 E. J. Yoo, J. Kim, E. Hosono, H. S. Zhou, T. Kudo and I. Honma, Nano Lett., 2008, 8, 2277.
4 K. R. Ratinac, W. R. Yang, S. P. Ringer and F. Braet, Environ. Sci. Technol., 2010, 44, 1167.
5 R. Arsat, M. Breedon, M. Shafiei, P. G. Spizziri, S. Gilje, R. B. Kaner, K. Kalantar-zadeh and W. Wlodarski, Chem. Phys. Lett., 2009, 467, 344.
6 J. D. Fowler, M. J. Allen, V. C. Tung, Y. Yang, R. B. Kaner and B. H. Weiller, ACS Nano, 2009, 3, 301.
7 I. Jung, D. Dikin, S. Park, W. W. Cai, S. L. Mielke and R. S. Ruoff, J. Phys. Chem. C, 2008, 112, 20264.
8 M. W. K. Nomania, R. Shishir, M. Qazi, D. Diwan, V. B. Shields, M. G. Spencer, G. S. Tompa, N. M. Sbrockey and G. Koley, Sens. Actuators, B, 2010, 150, 301.
9 Y. P. Dan, Y. Lu, N. J. Kybert, Z. T. Luo and A. T. C. Johnson, Nano Lett., 2009, 9, 1472.
10 W. J. Yuan, A. R. Liu, L. Huang, C. Li and G. Q. Shi, Adv. Mater. 2013, 25, 766.
11 W. W. Li, X. M. Geng, Y. F. Guo, J. Z. Rong, Y. P. Gong, L. Q. Wu, X. M. Zhang, P. Li, J. B. Xu, G. S. Cheng, M. T. Sun and L. W. Liu, ACS Nano, 2011, 5, 6955.
12 V. Tjoa, W. Jun, V. Dravid, S. Mhaisalkar and N. Mathews, J. Mater. Chem., 2011, 21, 15593.
13 G. Neria, S. G. Leonardi, M. Latino, N. Donatoc, S. Baek, D. E. Conte, P. A. Russo and N. Pinna, Sens. Actuators, B, 2013, 179, 61.
14 L. T. Hoa, H. N. Tien, V. H. Luan, J. S. Chung and S. H. Hur, Sens. Actuators, B, 2013, 185, 701.
15 X. Q. An, J. C. Yu, Y. Wang, Y. M. Hu, X. L. Yu and G. J. Zhang, J. Mater. Chem., 2012, 22, 8525.
16 J. Yi, J. M. Lee and W. I. Park, Sens. Actuators, B, 2011, 155, 264.
17 S. M. Liang, J. W. Zhu, C. Wang, S. T. Yu, H. P. Bi, X. H. Liu and X. Wang, Appl. Surf. Sci., 2014, 292, 278.
18 S. Z. Deng, V. Tjoa, H. M. Fan, H. R. Tan, D. C. Sayle, M. Olivo, S. Mhaisalkar, J. Wei and C. H. Sow, J. Am. Chem. Soc., 2012, 134, 4905.
19 N. Chen, X. G. Li, X. Y. Wang, J. Yu, J. Wang, Z. N. Tang and S. A. Akbar, Sens. Actuators, B, 2013, 188, 902.

20 X. Liu, J. S. Cui, J. B. Sun and X. T. Zhang, RSC Adv., 2014, 4, 22601.
21 S. M. Cui, Z. H. Wen, E. C. Mattson, S. Mao, J. B. Chang, M. Weinert, C. J. Hirschmugl, M. Gajdardziska-Josifovsk and J. H. Chen, J. Mater. Chem. A, 2013, 1, 4462.
22 Q. Q. Lin, Y. Li and M. J. Yang, Sens. Actuators, B, 2012, 173, 139.
23 Q. W. Huang, D. W. Zeng, H. Y. Li and C. S. Xie, Nanoscale, 2012, 4, 5651.
24 J. Zhang, C. Zhao, P. A. Hu, Y. Q. Fu, Z. l. Wang, W. W. Cao, B. Yang and F. Placido, RSC Adv., 2013, 3, 22185.
25 L. S. Zhou, F. P. Shen, X. K. Tian, D. H. Wang, T. Zhang and W. Chen, Nanoscale, 2013, 5, 1564.
26 G. W. Zhou, J. L. Wang, P. F. Gao, X. W. Yang, Y. S. He, X. Z. Liao, J. Yang and Z. F. Ma, Ind. Eng. Chem. Res., 2013, 52, 1197.
27 H. J. Song, X. H. Jia, N. Li, X. F. Yang and H. Tang, J. Mater. Chem., 2012, 22, 895.
28 S. Guo, G. K. Zhang, Y. D. Guo and J. C. Yu, Carbon, 2013, 60, 437.
29 X. F. Xia, Q. L. Hao, W. Lei, W. J. Wang, D.P. Sun and X. Wang, J. Mater. Chem., 2012, 22, 16844.
30 M. Y. Wang, T. Shen, M. Wang, D. E. Zhang, Z. W. Tong and J. Chen, Sens. Actuators, B, 2014, 190, 645.
31 Z. X. Jiang, J. Li, H. Aslan, Q. Li, Y. Li, M. L. Chen, Y. D. Huang, J. P. Froning, M. Otyepka, R. Zboril, F. Besenbacher and M.D. Dong, J. Mater. Chem. A, 2014, 2, 6714.
32 X. L. Cheng, Z. M. Rong, X. F. Zhang, Y.M. Xu, S. Gao, H. Zhao, L. H. Huo, Sens. Actuators, B, 2013, 188, 425.
33 L. H. Huo, Q. Li, H. Zhao, L. J. Yu, S. Gao, J. G. Zhao, Sens. Actuators, B, 2005, 107, 915.
34 W. S. Hummers and R. E. Offeman, J. Am. Chem. Soc., 1958, 80, 1339.
35 M. G. Chung, D. H. Kim, H. M. Lee, T. Kim, J. H. Choi, D. K. Seo, J. B. Yoo, S. H. Hong, T. J. Kang and Y. H. Kim, Sens. Actuators, B, 2012, 166–167, 172.
36 G. H. Lu, S. J. Park, K. H. Yu, R. S. Ruoff, L. E. Ocola, D. Rosenmann and J. H. Chen, ACS Nano, 2011, 5, 1154.
37 Y. Yao, X. D. Chen , H. H. Guo and Z. Q. Wu, Applied Surface Science, 2011, 257, 7778.
38 S. Mao, H. H. Pu and J. H. Chen, RSC Adv., 2012, 2, 2643.
39 K. N. Kudin, B. Ozbas, H. C. Schniepp, R. K. Prud'homme, I. A. Aksay and R. Car, Nano Lett., 2008, 8, 36.
40 H. L. Wang, J. T. Robinson, X. L. Li and H. J. Dai, J. AM. CHEM. SOC., 2009, 131, 9910.
41 G. I. Titelman, V. Gelman, S. Bron, R. L. Khalfin, Y. Cohen and H. Bianco-Peled, Carbon, 2005, 43, 641.
42 S. Stankovich, R. D. Piner, S. T. Nguyen and R. S. Ruoff, Carbon, 2006, 44, 3342.
43 M. B. Avinash, K. S. Subrahmanyam, Y. Sundarayya and T. Govindaraju, Nanoscale, 2010, 2, 1762.
44 G. K. Pradhan and K. M. Parida, ACS Appl. Mater. Interfaces, 2011, 3, 317.
45 N. S. McIntyre and D. G. Zetaruk, Anal.Chem., 1977, 49, 1521.
46 B. Hu, J. C. Yu, J. M. Gong, Q. Li and G. S. Li, Adv. Mater., 2007,19, 2324.
47 H. Feng, X. D. Wang and D. Z. Wu, Ind. Eng. Chem. Res., 2013, 52, 10160.
48 R. K. Joshi, H. Gomez, F. Alvi and A. Kumar, J. Phys. Chem. C, 2010, 114, 6610.
49 D. H. Yoon and G. M. Choi, Sens. Actuators, B, 1997, 45, 251.
50 S. M. Cui, H. H. Pu, E. C. Mattson, G. H. Lu, S. Mao, M. Weinert, C. J. Hirschmugl, M. Gajdardziska-Josifovskab and J. H. Chen, Nanoscale, 2012, 4, 5887.

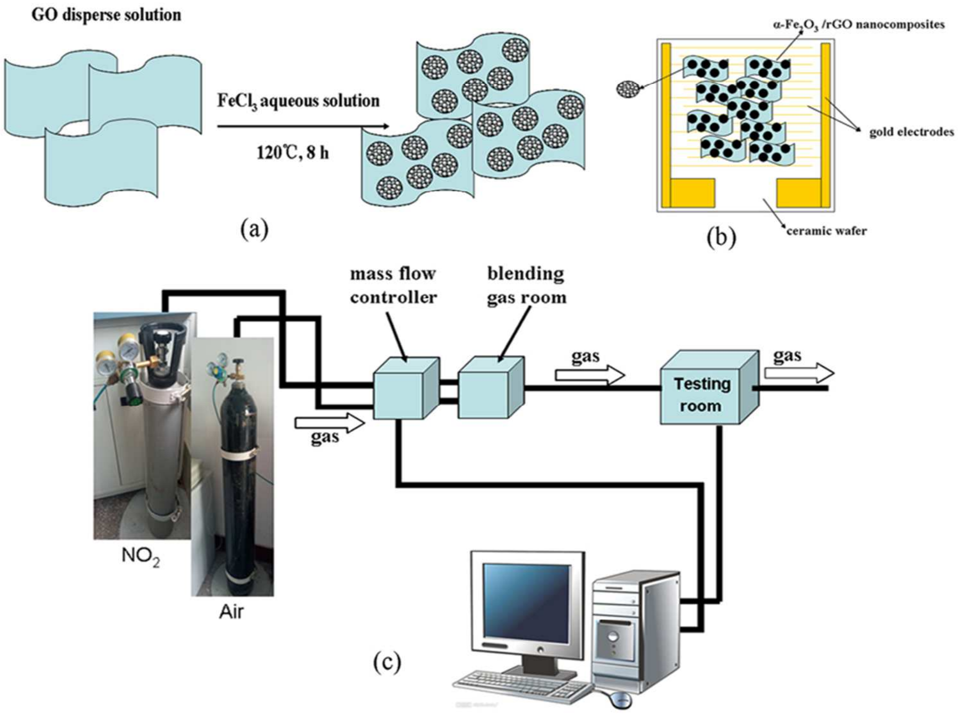


Fig. 1 The experimental reaction diagram of α-Fe2O3/rGO nanocomposites (a), schematic of α-Fe2O3/rGO nanocomposites on the sensor substrate (b) and schematic of sensing test (c).
80x60mm (300 x 300 DPI)

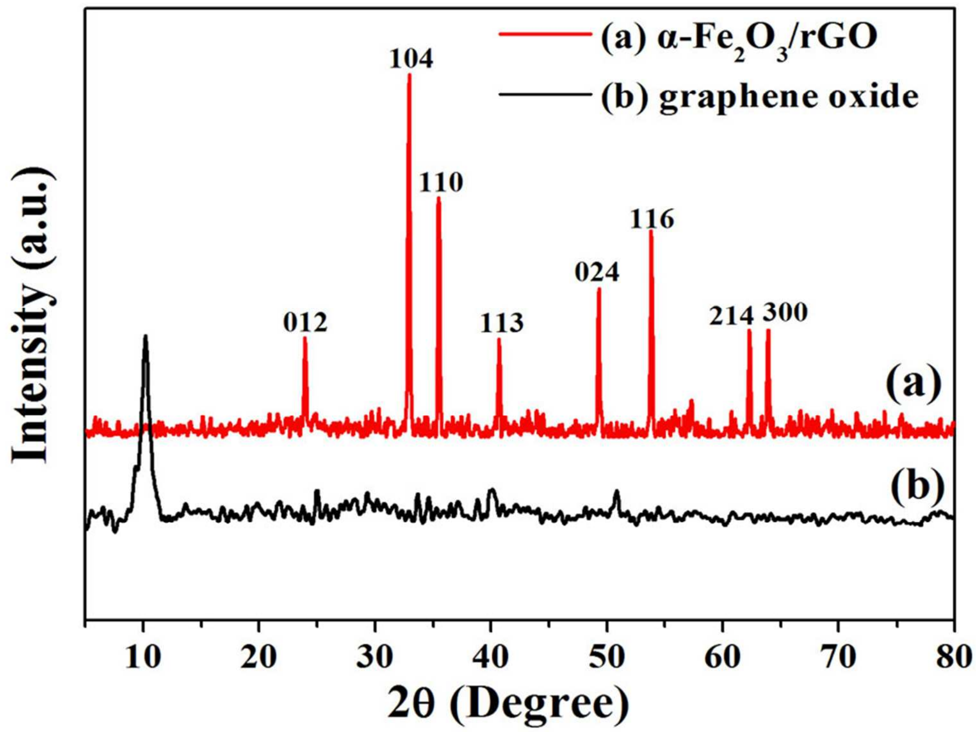


Fig. 2 XRD patterns of α-Fe2O3/rGO nanocomposites (a) and graphene oxide (b).
80x60mm (300 x 300 DPI)

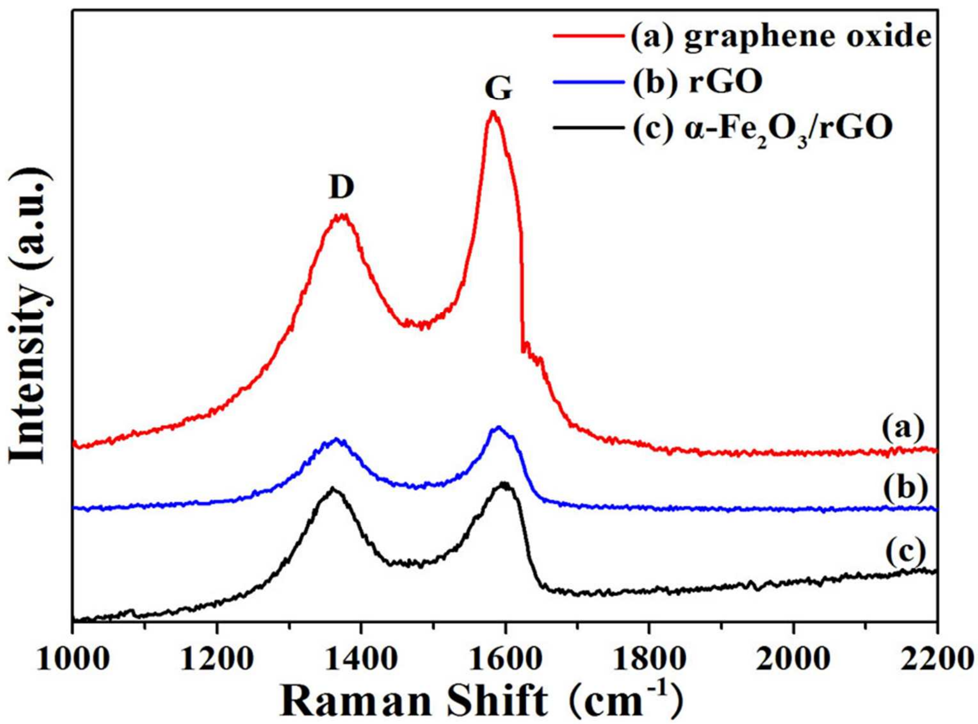


Fig. 3 Raman spectra of graphene oxide (a), reduced graphene oxide (rGO) (b) and α-Fe2O3/rGO nanocomposites (c).
80x60mm (300 x 300 DPI)

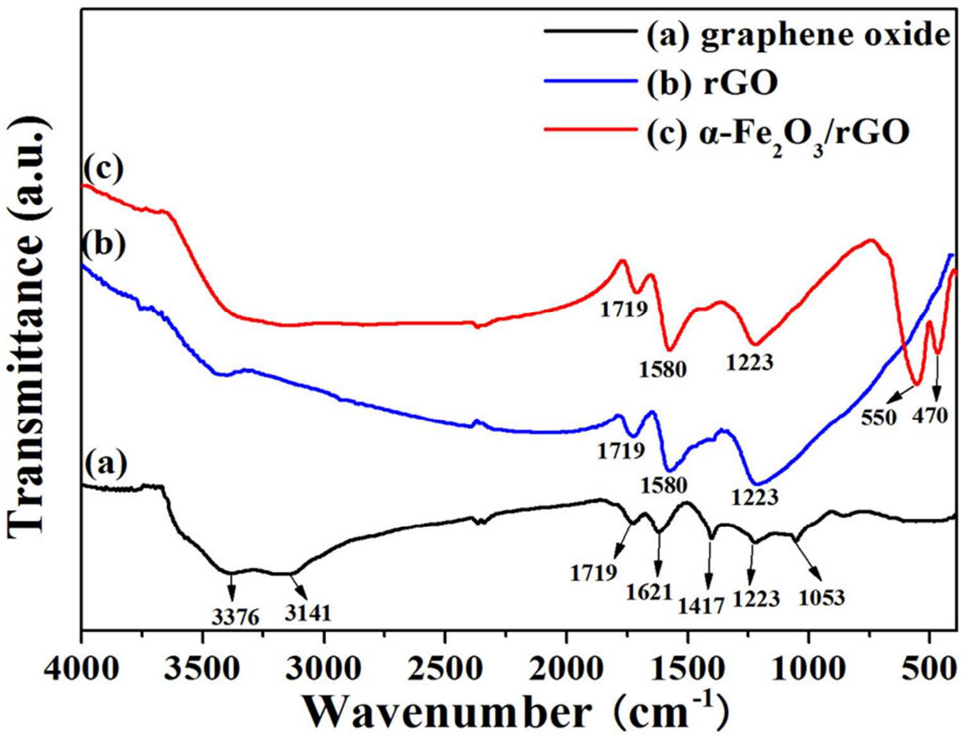


Fig. 4 FT-IR spectra of graphene oxide (a), rGO (b) and α-Fe2O3/rGO nanocomposites (c).
80x60mm (300 x 300 DPI)

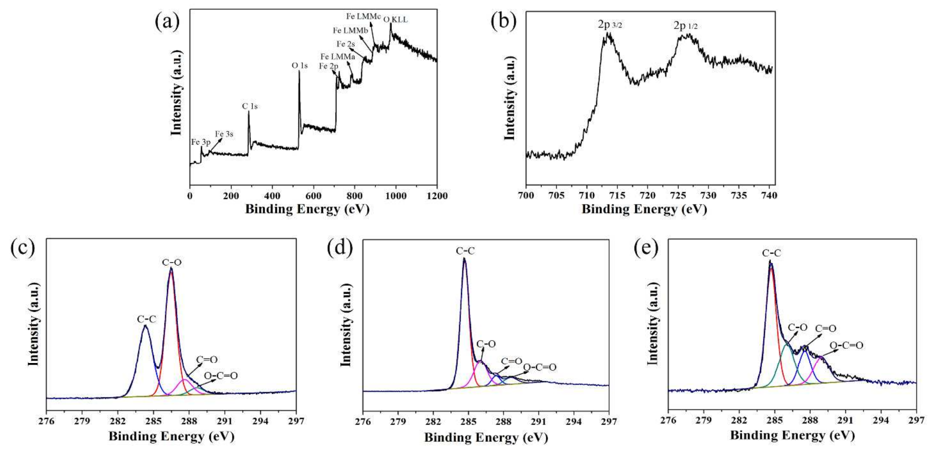


Fig. 5 XPS spectra of full survey (a), the fine spectrum of Fe2p (b), the fine spectrum of C 1s of graphene oxide (c), reduced graphene oxide (d) and α-$Fe_2O_3$/rGO nanocomposites (e).
279x139mm (300 x 300 DPI)

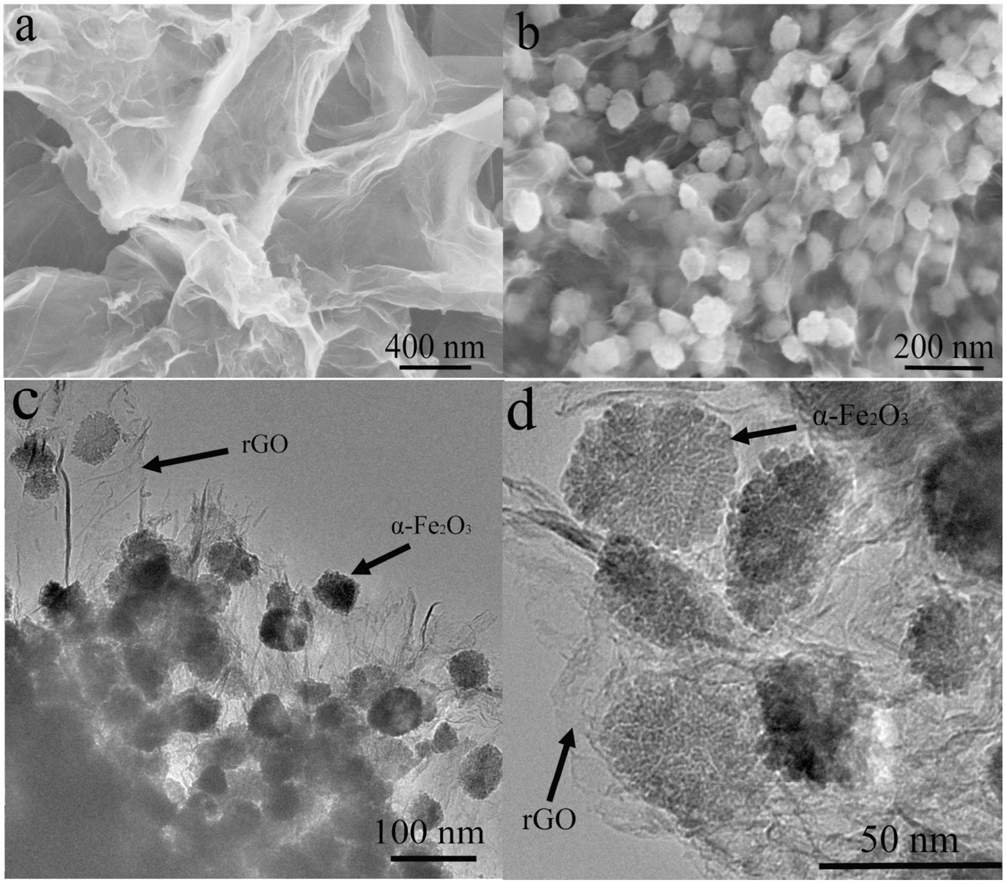


Fig. 6 SEM images of reduced graphene oxide (a) and α-Fe2O3/rGO nanocomposites (b). TEM images of α-Fe2O3/rGO nanocomposites (c-d).
160x140mm (300 x 300 DPI)

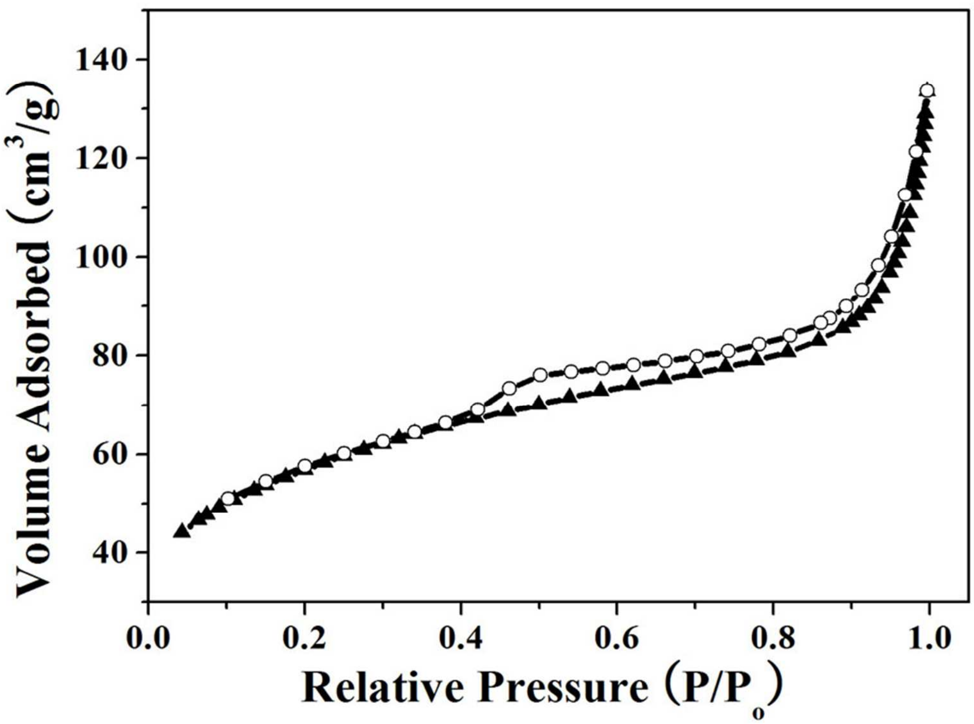


Fig. 7 Nitrogen adsorption–desorption isotherm of α-Fe2O3/rGO nanocomposites.
80x60mm (300 x 300 DPI)

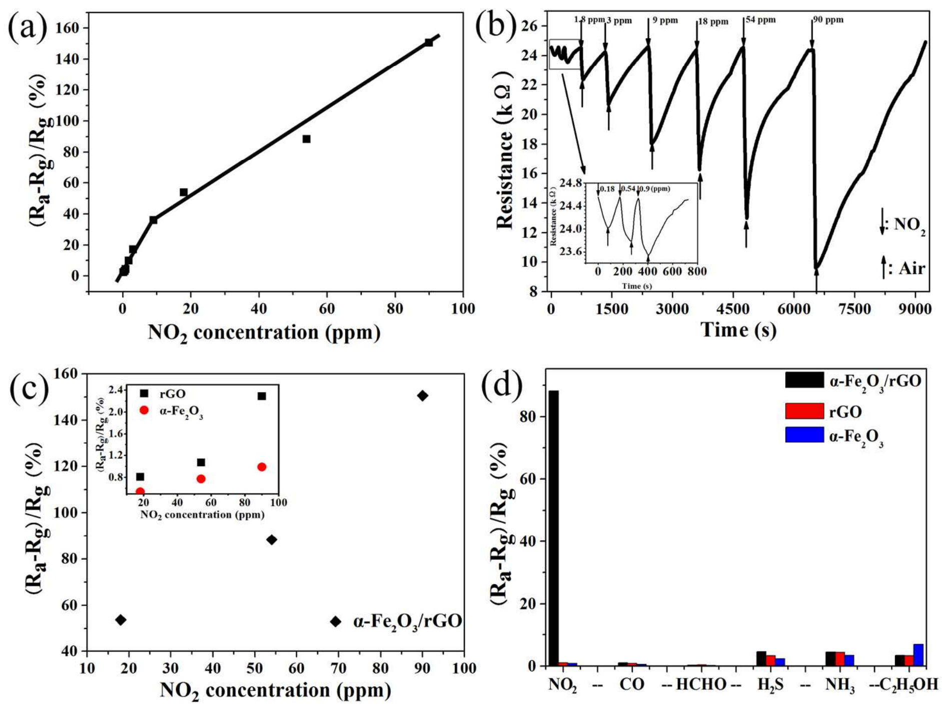


Fig. 8 (a) Exponential curve of response of the nanocomposites as a function of NO2 concentration. (b) Dynamic responses of α-Fe2O3/rGO nanocomposites to different concentrations of NO2. (c) Response comparison of α-Fe2O3/rGO nanocomposites, reduced graphene oxide and α-Fe2O3 to 18～90 ppm NO2. (d) Response comparison of α-Fe2O3/rGO nanocomposites, reduced graphene oxide and α-Fe2O3 to different gases.
173x130mm (300 x 300 DPI)

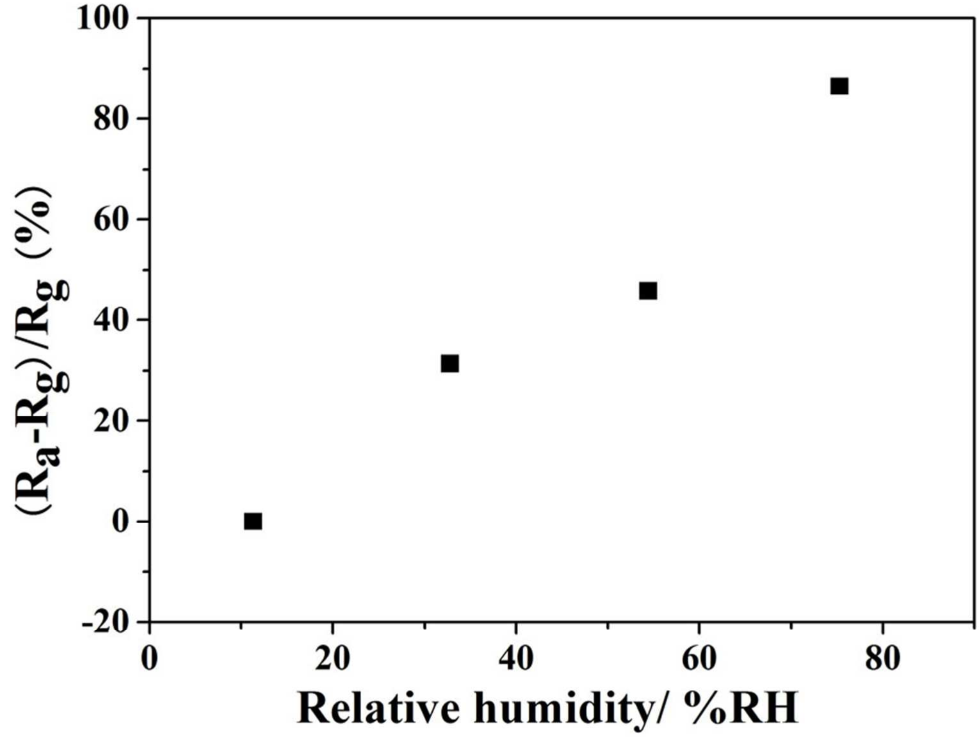


Fig. 9 Responses of α-Fe2O3/rGO nanocomposites to humidity from 11.3 to 75.3% RH at room temperature.
80x60mm (300 x 300 DPI)

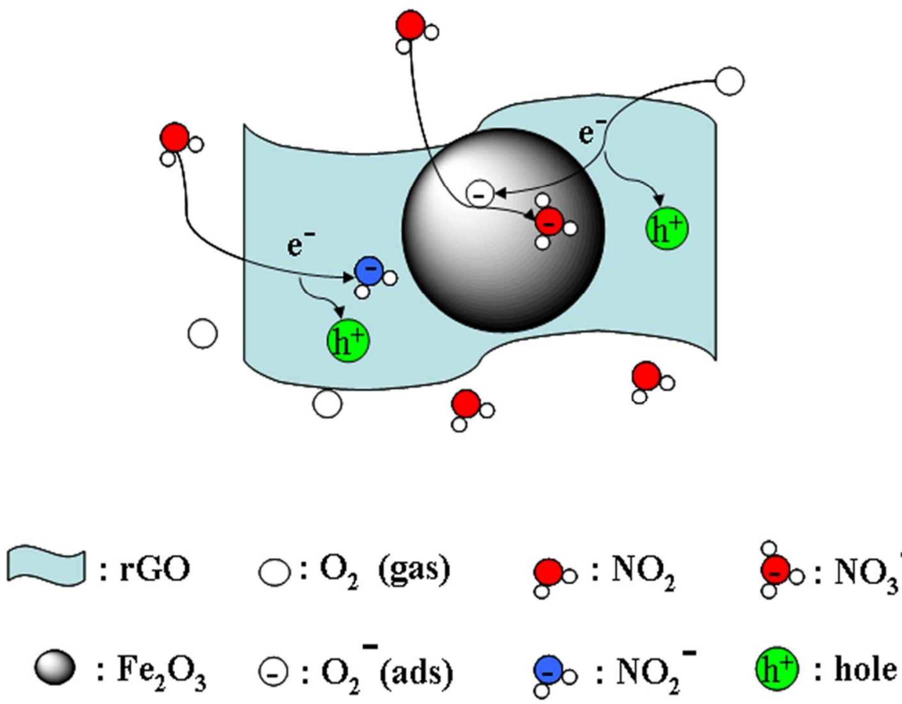


Fig. 10 Proposed sensing mechanism of α-Fe2O3/rGO nanocomposites to NO2.
80x60mm (300 x 300 DPI)

**Table 1:** Standard equilibrium relative humidity at the confined space on the top of saturated salt solutions at room temperature (25 ℃).

| **Salt** | **LiCl** | **$MgCl_2$** | **$Mg(NO_3)_2$** | **NaCl** |
|---|---|---|---|---|
| **Humidity (% RH)** | **11.3** | **32.8** | **54.4** | **75.3** |

**Table 2:** The percent contents of chemical states of C 1s (%) in graphene oxide, rGO and α-$Fe_2O_3$/rGO nanocomposites.

| **Materials** / **The chemical states of C 1s (%)** | **C－C** | **C－O** | **C=O** | **O－C=O** |
|---|---|---|---|---|
| **graphene oxide** | **39.86** | **50.4** | **5.64** | **4.09** |
| **rGO** | **88.5** | **7.64** | **1.87** | **1.99** |
| **α-$Fe_2O_3$/rGO nanocomposites** | **50.12** | **25.59** | **13.91** | **10.37** |

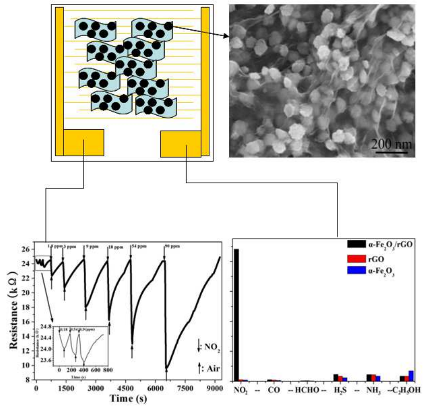


Highly selective $NO_2$ sensor at room temperature based on the hierarchical nanosphere-like $\alpha$-$Fe_2O_3$ modified rGO nanocomposites were developed by a simple hydrothermal method without any surfactant or template.